

High temperature mid-IR polarizer via natural in-plane hyperbolic Van der Waals crystals

Nihar Ranjan Sahoo,^{1,*} Saurabh Dixit,^{1,*} Anuj Kumar Singh,¹
Sang Hoon Nam,² Nicholas X. Fang,^{2,†} and Anshuman Kumar^{1,‡}

¹*Laboratory of Optics of Quantum Materials, Physics Department,
Indian Institute of Technology Bombay, Mumbai - 400076, India*

²*Department of Mechanical Engineering, Massachusetts Institute of Technology, Cambridge, MA-02139, USA*

(Dated: August 29, 2021)

Integration of conventional mid to long-wavelength infrared polarizers with chip-scale platforms is restricted by their bulky size and complex fabrication. Van der Waals materials based polarizer can address these challenges due to its non-lithographic fabrication, ease of integration with chip-scale platforms, and room temperature operation. In the present work, mid-IR optical response of the sub-wavelength thin films of α -MoO₃ is investigated for application towards high temperature mid-IR transmission and reflection type thin film polarizer. To our knowledge, this is the first report of above room temperature mid-IR optical response of α -MoO₃ to determine the thermal stability of the proposed device. We find that our α -MoO₃ based polarizer retains high extinction ratio with peak value exceeding 10 dB, up to a temperature of 140°C. We explain our experimental findings by natural in-plane hyperbolic anisotropy of α -MoO₃ in the mid-IR, high temperature X-ray diffraction and Raman spectroscopic measurements. This work opens up new avenues for naturally in-plane hyperbolic van der Waals thin-films to realize sub-wavelength IR optical components without lithographic constraints.

Keywords: Hyperbolic in-plane anisotropy, natural hyperbolic materials, van der Waals crystal, 2D materials, mid-IR polarizer

I. INTRODUCTION

Recently, a new class of van der Waals (vdW) layered materials have been shown to possess natural hyperbolic anisotropy in mid-infrared (IR) spectral region[1–4]. Hyperbolic anisotropy is an extreme type of optical anisotropy in which the real part of dielectric permittivity holds the opposite sign in different crystallographic directions. As a result, within a hyperbolic spectral region, the vdW material behaves like a metal in one crystal direction and a dielectric in the other crystal direction. Unlike artificial hyperbolic metamaterials[5]—where in-plane hyperbolic anisotropy is invoked by lithographic patterning, natural hyperbolicity of these vdW materials is attributed to structural anisotropy of crystal unit cell. In particular, h-BN[3], α -MoO₃[1, 6] and α -V₂O₅[2] are natural hyperbolic materials (NHMs) which exhibit Restrahlen Bands (RBs)—the spectral region between longitudinal optical (LO) and transverse optical (TO) phonons - in the mid-IR spectral region and show hyperbolicity due to interaction of optical phonons with photons (light-matter interaction). Phonons have a relatively long lifetime compared to plasmons resulting in lower optical losses than their analogous plasmonic-based metamaterials[7–9] in which photons are coupled with plasmons. Many NHMs [1–3] exhibit hyperbolic anisotropy in mid-IR spectral region (3 μ m - 30 μ m) which

has diverse applications like polarized IR imaging[10], molecular sensing[11, 12], free space communication[13] and quantum interference[14]. Unlike h-BN, which possesses uniaxial hyperbolic anisotropy (i.e. $\epsilon_{xx} = \epsilon_{yy} \neq \epsilon_{zz}$), α -MoO₃ exhibits in-plane hyperbolic anisotropy (i.e. $\epsilon_{xx} \neq \epsilon_{yy} \neq \epsilon_{zz}$) which is particularly beneficial for planar mid-IR optical devices[15, 16]. With this motivation, there has been recent interest in developing flat optics based on vdW layered materials which can be integrated with chip-scale platforms using vdW integration, operational at room temperature, and does not involve complex lithographic fabrication techniques[17–20].

We present an application of α -MoO₃ in the mid-IR spectral region, i.e. from 545⁻¹ - 1000 cm⁻¹ (around 10 μ m - 18 μ m), as a thin film polarizer that reflects the light with one state of polarization while transmitting the light with its orthogonal state of polarization. Here, single-crystal α -MoO₃ thin films are synthesized using physical vapor deposition (schematically shown in Fig. 1(a)) and are transferred on top of potassium bromide (KBr) window, purchased from Edmund Optics, using mechanical exfoliation technique. In-plane anisotropy of the synthesized α -MoO₃ thin film is confirmed using polarization-resolved Raman spectroscopy. We optimize the mid-IR optical responses of α -MoO₃, mainly transmittance and reflectance, as a function of the thickness. Optimum thickness of α -MoO₃ based IR polarizer is found to lie in the range of 2.5 μ m - 3.5 μ m for which the extinction ratio (ER) is obtained more than 7.5 dB and 10 dB in a broad mid-IR spectral region, respectively for reflection and transmission geometry with remarkable operational bandwidth and degree of polarization (DOP) in long-wavelength IR regime. Moreover, to the

* These two authors contributed equally

† nicfang@mit.edu

‡ anshuman.kumar@iitb.ac.in

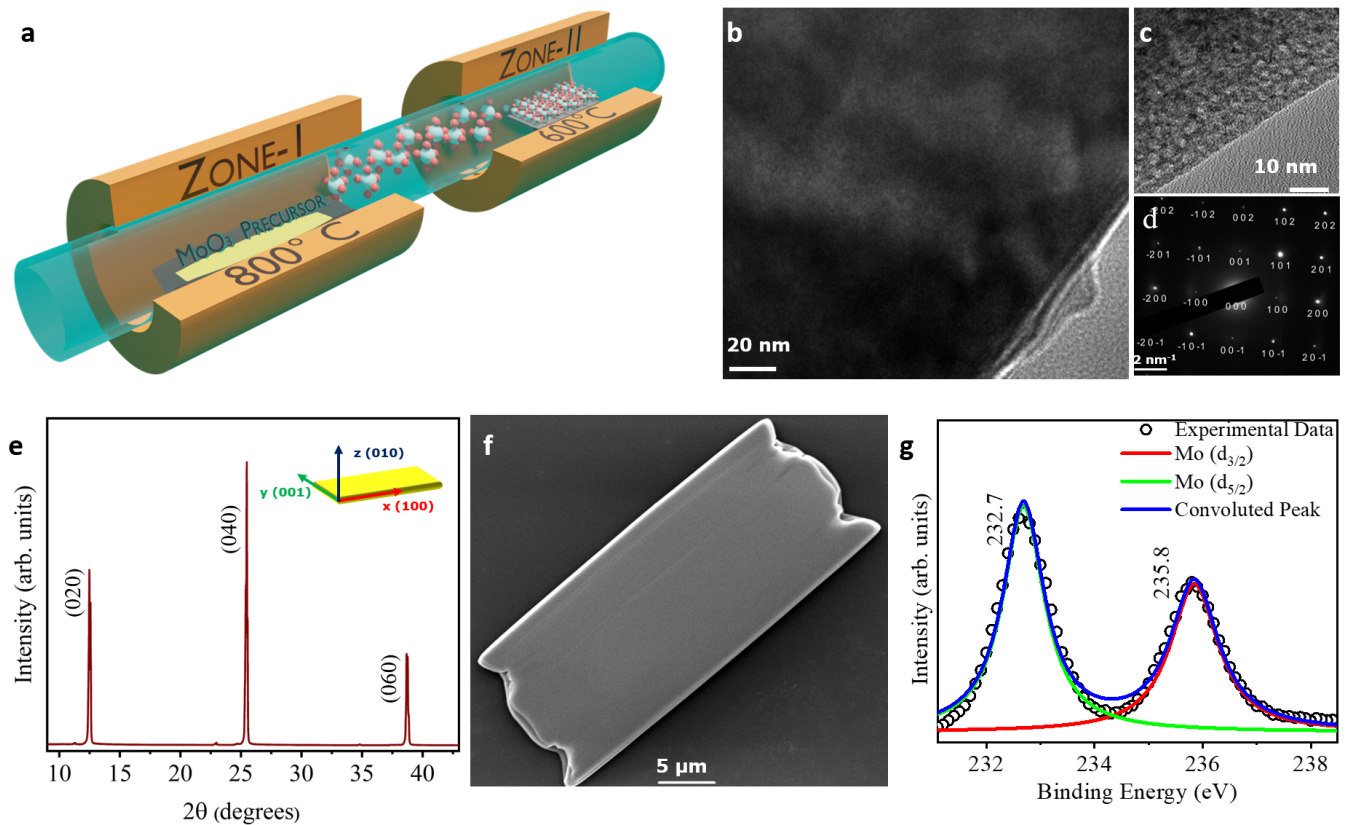


FIG. 1. **Structural and chemical properties of fabricated α -MoO₃ thin films.** (a) Schematic illustration of thermal physical deposition technique for fabrication of α -MoO₃ thin films. (b)-(c) High-resolution transmission electron microscopic images and (d) selected area electron diffraction pattern of the fabricated α -MoO₃ thin film. (e) X-ray Diffraction of α -MoO₃ thin films (inset shows the crystallographic direction of α -MoO₃ planes with the coordinate axes). (f) A representative scanning electron microscopic image of as-deposited α -MoO₃ thin films on a silicon substrate. (g) X-ray Photoelectron Spectroscopy of α -MoO₃ thin film where the scattered plots represent the experimental data and solid lines are the fitted data for the binding energies of Mo $d_{5/2}$ and Mo $d_{3/2}$.

best of our knowledge, this is the first work where the optical response of α -MoO₃ is studied above room temperature, to determine the operating temperature tolerance for the α -MoO₃ thin-film based polarizer device. We observe that the ER and DOP of α -MoO₃ thin films retain their values up to a temperature of 140 °C. We explain these experimental results through extensive full wave simulations of Maxwell's equations and via complementary measurements using temperature dependent X-ray diffraction and Raman spectroscopy.

II. RESULTS AND DISCUSSION

We first confirm the structure of our fabricated crystals. Representative high-resolution transmission electron microscopy (HRTEM) and selected area electron diffraction (SAED) analysis of synthesized thin films are shown in Fig. 1(b)-(d). The estimated values of in-plane lattice constants are around 3.69 Å and 3.97 Å. Further structural information of synthesized thin films is investigated via X-Ray diffraction pattern (shown in Fig. 1(e))

which shows sharp diffraction peaks at the 2θ values of 12.48°, 25.48° and 38.76° corresponding respectively to (020), (040), and (060) planes of α -MoO₃ [21]. Out of plane lattice constant is found around 14.14 Å using Bragg's Law[22]. The values of lattice constants evaluated from XRD, HRTEM, and SAED match closely with the lattice parameters of the orthorhombic phase of MoO₃ (i.e. α -MoO₃)[1, 21]. SEM image of the synthesized α -MoO₃ thin films on the silicon substrate is shown in Fig. 1(f), which reveals the rectangular shape of flake. Chemical composition of the thin films is examined using X-ray photoelectron spectroscopy. XPS spectrum exhibits binding energies of Mo 3d doublets at 232.7 eV (for $3d_{5/2}$) and 235.8 eV (for $3d_{3/2}$) which is associated with the VI oxidation state of molybdenum (Fig. 1(g)). These peaks indicate negligible oxygen vacancies in the synthesized α -MoO₃ thin films[23]. These investigations substantiate the fact that the chemical and structural properties of our fabricated rectangular-shaped α -MoO₃ thin films using thermal physical deposition technique are as expected.

Next, we explore the anisotropy of α -MoO₃ thin films

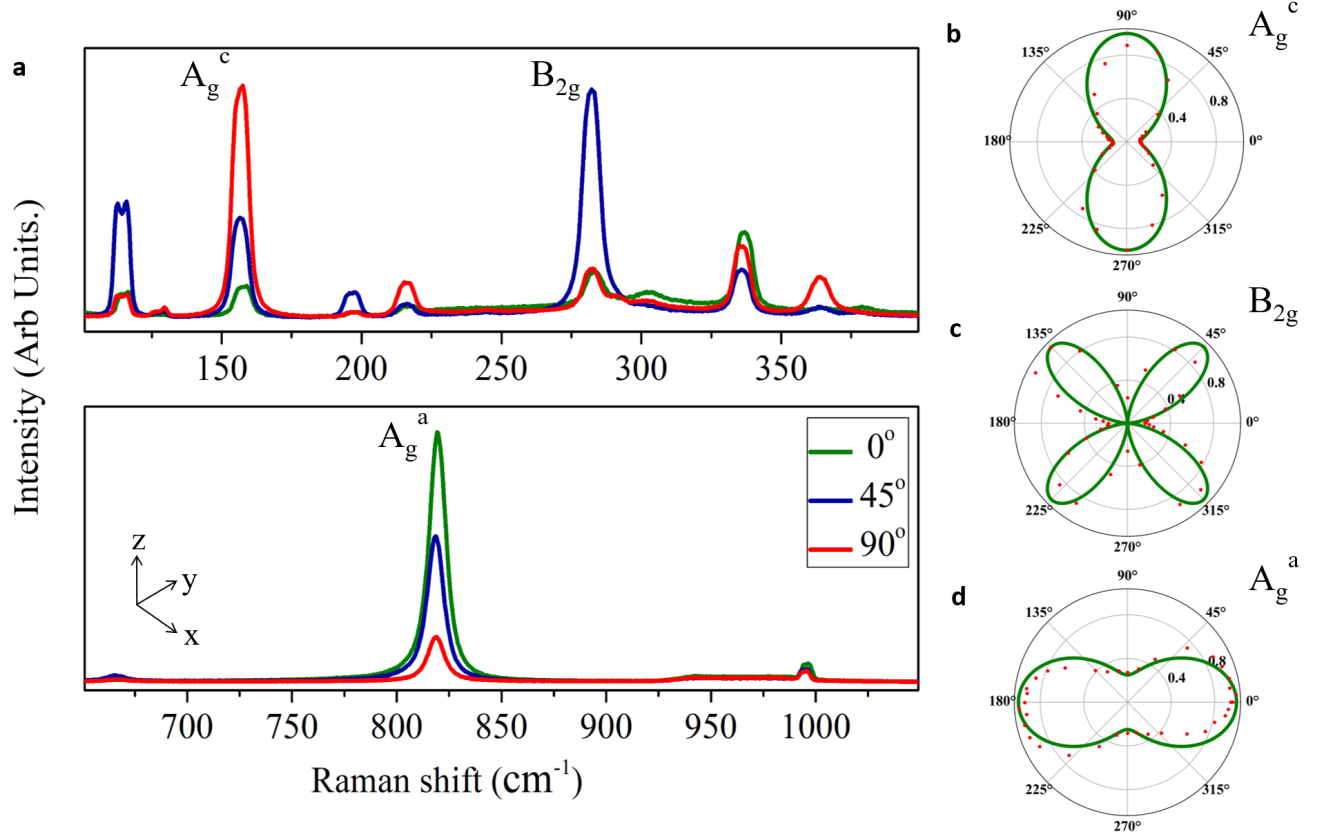


FIG. 2. **Polarization resolved Raman scattering spectroscopy.** (a) Polarization resolved raman spectra of α - MoO_3 thin film at $\beta \sim 0^\circ$ (green), 45° (blue) and 90° (red) exhibiting characteristic phonon energies of α - MoO_3 . Polar plot of angle resolved normalized Raman intensities for (b) A_g^c , (c) B_{2g} and (d) A_g^a modes of α - MoO_3 .

using polarization-resolved Raman spectroscopy. The α - MoO_3 unit cell follows the D_{2h}^{16} space group [24] which consists of 4 Mo and 12 O (total 16 atoms). Hence, there are 48 phonon modes at the center of the Brillouin zone having the following decomposition[25]:

$$\begin{aligned} \Gamma^{\text{vib}} = & 8A_g \oplus 4B_{1g} \oplus 4B_{2g} \oplus 8B_{3g} \oplus 4A_u \\ & \oplus 7B_{1u} \oplus 7B_{2u} \oplus 3B_{3u} \end{aligned}$$

Out of these modes, A_g , B_{1g} , B_{2g} , and B_{3g} are Raman active modes. Since α - MoO_3 has an orthorhombic crystal structure, it has different Raman active modes associated with phonons along different crystallographic directions. Here, we focus on the B_{2g} mode (at 282 cm^{-1}) which is the wagging mode of O-Mo-O atoms, A_g mode for the translational vibration of MoO_6 chain along the y - crystal direction (called A_g^c mode) at 157 cm^{-1} , and A_g mode from asymmetric stretching of O-Mo-O atoms along the x - crystal direction is at 818 cm^{-1} (called A_g^a mode)[26]. If e_i and e_s are the polarization unit vectors along the incident and scattered light, then Raman intensity is given by $I \propto |e_i \cdot R \cdot e_s|^2$. The angular dependence of the Raman intensity for A_g and B_{2g} modes

can be obtained from:

$$R(A_g) = \begin{pmatrix} A & 0 & 0 \\ 0 & B & 0 \\ 0 & 0 & C \end{pmatrix}$$

$$R(B_{2g}) = \begin{pmatrix} 0 & 0 & E \\ 0 & 0 & 0 \\ E & 0 & 0 \end{pmatrix}$$

Here, A , B , C and E represent the strength of Raman tensor's elements. Intensity of these Raman modes can be theoretically captured via the Raman tensor[24] as:

$$\begin{aligned} I(A_g) & \propto (A \cos^2 \beta + B \sin^2 \beta)^2 \\ I(B_{2g}) & \propto E^2 \sin^2 2\beta \end{aligned} \quad (1)$$

Here, β represents the angle between the $[100]$ crystal direction and the polarization state of laser. In Fig. 2(a), our experimental Raman spectra show A_g^c , B_{2g} and A_g^a modes at 156 cm^{-1} , 282 cm^{-1} , and 818 cm^{-1} respectively for $\beta \sim 0^\circ$, 45° and 90° . These characteristic Raman modes of α - MoO_3 show a variation in the Raman

intensities as a function of β , which is attributed to the dependence of Raman intensity tensor on the polarization state of incident laser light and the crystallographic directions. Fig. 2(b)-(d) present polar plots for theoretical and experimental Raman intensities of A_g^c , B_{2g} and A_g^a respectively. Theoretical variation of Raman intensities of these modes is calculated using Eq. 1. B_{2g} mode has the angular periodic intensity variation of 90° (four lobes), and the orientation of two-lobed A_g modes are orthogonal to each other. For A_g^c and A_g^a mode, the ratio of A and B are taken as 0.35 and 2 in the Eq.1, respectively, to fit our experimental polarization-resolved Raman data. Here, the condition $A > B$ results in the formation of a two-lobed main axis parallel to the x -axis (i.e. [100] direction). On the other hand, $A < B$ leads to a two-lobed main axis perpendicular to the x -axis. These results validate that synthesized α -MoO₃ flakes exhibit the expected crystallographic orientation with strong in-plane anisotropy, which is crucial for the functioning of our proposed IR polarizer.

The optical response of a thin film depends on its thickness and hence it is a vital parameter for the polarizer. Therefore, we consider different thicknesses of α -MoO₃ thin film from the flakes transferred using mechanical exfoliation technique and investigate their mid-IR optical responses. Thicknesses of α -MoO₃ thin films are measured using a profilometer and are shown in Fig. S2 of the supplementary information for three representative samples D1, D2, and D3, respectively. The mechanical exfoliation technique results in the transfer of vdW flakes with non-uniform thicknesses. For instance for samples D1, D2 and D3 thicknesses are found to be in the range 2.27-3.08 μm , 2.64-3.53 μm and 3.95-4.59 μm respectively.

Next, we explore the mid-IR optical responses of α -MoO₃ thin films. α -MoO₃ exhibits three RBs in the spectral range of 544.6 cm^{-1} to 850.1 cm^{-1} (RB-1), 821.4 cm^{-1} to 963 cm^{-1} (RB-2), and 956.7 cm^{-1} to 1006.9 cm^{-1} (RB-3), where the real part of dielectric permittivity is negative along [001], [100] and [010] crystal direction of α -MoO₃ respectively[27]. Due to the in-plane hyperbolic anisotropy of α -MoO₃ along [100] and [001] crystallographic directions in the RBs, α -MoO₃ reflects light which is linearly polarized along one direction. In contrast, the light with an orthogonal polarization state gets transmitted as shown schematically in Fig. 3(a). Hence, α -MoO₃ exhibits anisotropic reflectance and transmittance for s - and p - polarized light in the RB-1 and RB-2, respectively, making it a suitable candidate for reflecting as well as transmitting type mid-IR polarizer.

We validate this concept using a finite element method based on full-wave numerical simulation, COMSOL MULTIPHYSICS[28], for a representative thickness of 2.5 μm . We plot the magnitude of normalized electric field distribution at the frequency 620 cm^{-1} (i.e. RB-1) for incident electric field polarization along [100] and [001] crystal directions of α -MoO₃ (shown in Fig. S3 of supplementary information). When the incident electric field is along [001] direction (s -polarized), it is majorly reflected by

α -MoO₃, and a small amplitude of the incident light is transmitted. In contrast, when the incident electric field is along [100] direction (p -polarized), a small amplitude of the incident electric field is reflected by α -MoO₃ and majorly transmits the incident electric field. We further develop a transfer matrix method (TMM) based semi-analytical model to estimate the optical responses for p - and s - polarized light incident on α -MoO₃ as a function of thickness and frequency. Details of the model parameters with reflectance and transmittance color plots are provided in supplementary information Sec. S1. The findings from TMM corroborate our numerical simulation results. To quantify the performance of α -MoO₃ based polarizer, we define extinction ratio (ER) as

$$ER = 10 \log \frac{I_p}{I_s} \quad (2)$$

where I_p and I_s are the reflectances (transmittances) of p -polarized and s -polarized light respectively. Fig. 3(b)-(c) presents ER as a function of thickness and frequency for reflected and transmitted light, respectively, which are calculated using the TMM approach. Optimum thickness of the α -MoO₃ based polarizer for large ER and bandwidth is found to be in the range of 2.5 μm to 3.5 μm . Corresponding theoretical reflectances and transmittances color plots as a function of frequency and thickness have been shown in Fig. S4 of supplementary information. At higher α -MoO₃ thicknesses, Fabry-Perot (FP) modes appear for p -polarized incident light within RB-1 spectral region[29]. Furthermore, the theoretical transmittance for s - polarized light in RB-1 spectral region is significantly small (0.001) obtaining which is practically difficult due to noise. Therefore, a reduction of experimental ER is expected in the RB-1 spectral region for transmission as well reflection mode.

Fig. 3(d)-(e) represents the ER and DOP, respectively obtained from the experimentally observed polarization-resolved reflectance and transmittance micro-FTIR spectra. These polarization resolved reflectance and transmittance spectra for samples D1 - D3 are shown in Fig. S4 and Fig. S5 of supplementary information. It is worth mentioning that experimentally observed reflectance and transmittance spectra show some deviation from their theoretical counterpart (Fig. S3 of supplementary information). This discrepancy is attributed to multiple factors. Firstly, there are optical losses in the KBr substrate due to contamination from the flake transfer method. Secondly, we obtain a range of thicknesses from the mechanical exfoliation technique. Since FP modes, observed for p - polarized light in RB-1 spectral region, strongly depend on the thickness of α -MoO₃, range of thickness might lead to modulation of FP modes and consequently the optical responses for p - polarized light in RB-1 spectral region. Hence the theoretical spectrum deviates from the experimental spectrum. We believe that with an improvement in transfer technique, this discrepancy can be resolved and some performance metrics close to the theoretical limit can be obtained.

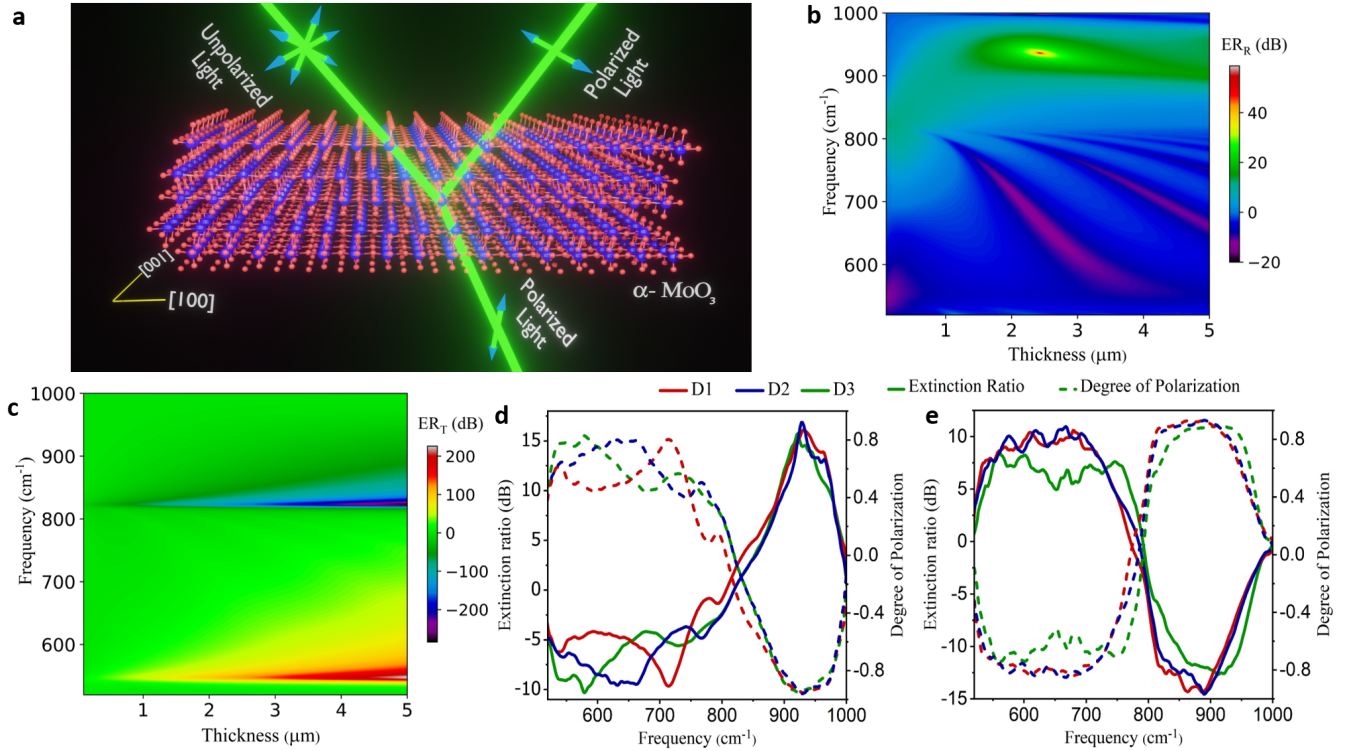


FIG. 3. **Figures of merit of mid-IR polarizer in the transmission and reflection geometry.** (a) Schematic illustration of α -MoO₃ thin film as a reflecting and transmitting type polarizer device. (b) - (c) shows theoretical ER as a function of thickness and frequency for reflected and transmitted light respectively. (d) - (e) represent the ER and DOP of IR polarizer based on α -MoO₃ thin films in reflection and transmission geometry, respectively, for Samples D1 - D3. Solid lines and dashed lines correspond to ER and DOP respectively.

Samples	Reflection Bandwidth (cm ⁻¹)		Transmission Bandwidth (cm ⁻¹)	
	RB-1	RB-2	RB-1	RB-2
D1	694 - 731	892- 977	545 - 726	810 - 924
D2	571 - 678	900 - 977	545 - 726	815 - 928
D3	545 - 613	892 - 972	586 - 608	847 - 948

TABLE I. Operational bandwidth for Samples D1 - D3 in both RBs of α -MoO₃ in reflection and transmission geometry.

To evaluate the operational bandwidth of the proposed IR polarizer, we chose characteristic parameters like ER, so that the experimentally occurred optical losses are compensated in both polarization states of light and give us realistic operational parameters. The ER thresholds for RB-1 and RB-2 spectral regions are considered as 7.5 dB and 10 dB, respectively, to evaluate the operational bandwidth. In the reflection geometry (Fig. 3(d)), a shift of operational spectral bandwidth is observed in the ER spectra towards lower frequency as we go from flake D1 to D3. This is due to the higher thicknesses of α -MoO₃ from flake D1 to D3, which leads to the change in frequency of FP modes in the RB-1 spectral region resulting in the shift of operational bandwidth in the RB-1 spectral region. Optimum thickness is closest to that of sam-

ple D2, which provides a larger operational bandwidth ($2.75\mu\text{m}$) compared to D1 ($0.73\mu\text{m}$) and D3 ($2.04\mu\text{m}$) in the RB-1, a trend which is consistent with our theoretical predictions. However, we observe no significant change in the operational bandwidth in the RB-2 spectral region for samples D1 - D3 and operational bandwidth is found around $1.0\mu\text{m}$. Furthermore, the DOP spectrum, given by $(I_s - I_p)/(I_s + I_p)$, is also shown for D1 - D3 in Fig. 3(d). The DOP informs us about the state of polarization of output light in which ± 1 represents completely polarized light, and 0 represents unpolarized light. In the proposed operational bandwidths, DOP is observed to be more than 0.75 and -0.85 in RB-1 and RB-2, respectively, suggesting nearly linear polarized light at the output. In our configuration, \pm signs in DOP correspond to s - and

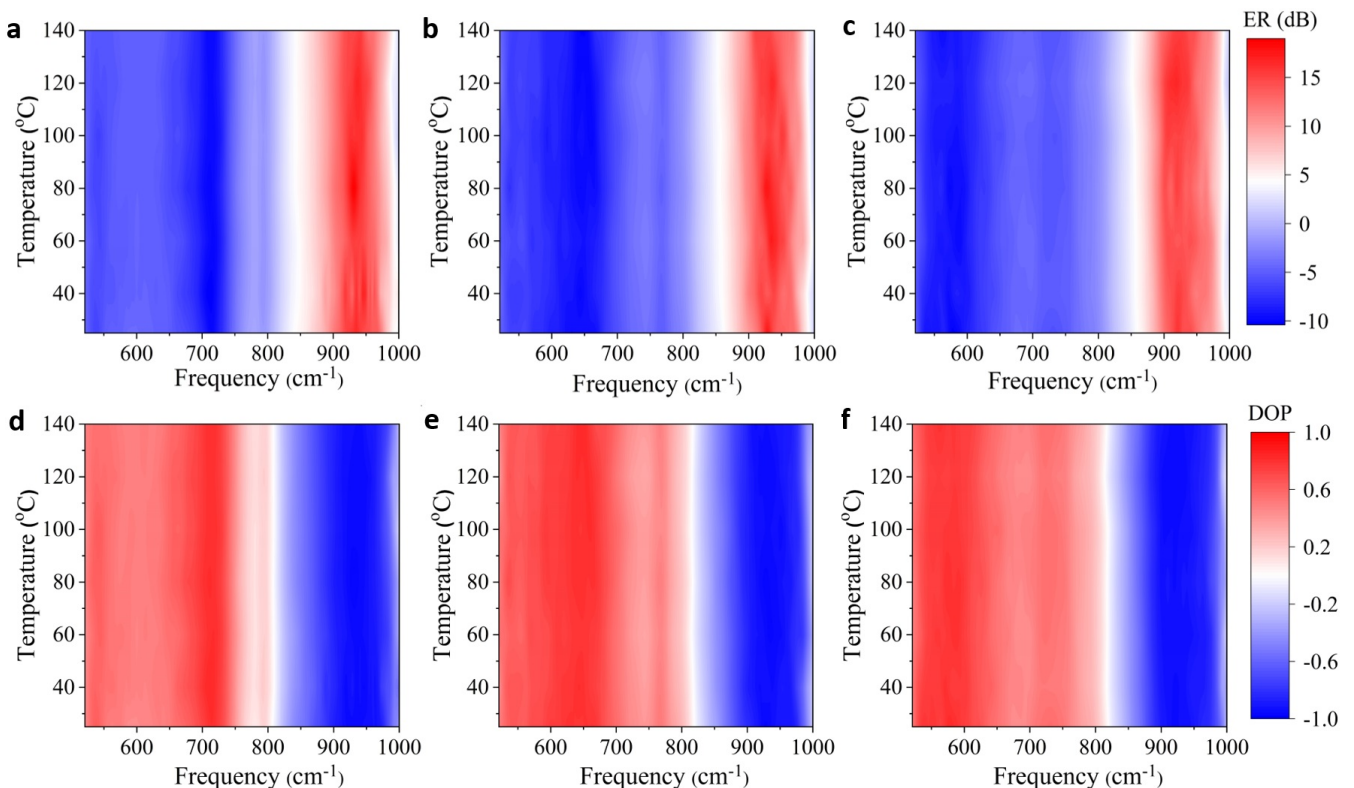


FIG. 4. **Temperature-dependent figures of merit of α -MoO₃ based IR polarizer in reflection geometry.** (a)-(c) show ER as a function of frequency and temperature for thicknesses D1, D2, and D3 respectively. (d)-(f) show DOP as a function of frequency and temperature for thicknesses D1, D2, and D3 respectively.

p - polarisation state of output light respectively.

Experimentally measured figures of merit in transmission geometry, displayed in Fig. 3(e), show almost similar bandwidths for samples D1 and D2 for ER values of 7.5 dB and 10 dB in RB-1 and RB-2, respectively. However, ER remains below 7.5 dB in most of RB-1 for D3. This is because sample D3 majorly consists of flakes with thickness around $4.0\mu\text{m}$, which is suboptimal, as discussed earlier. FP modes in the higher thicknesses lead to increased absorption of p - polarized light in RB-1 and result in the reduction of transmittance, which is evident from reflectance and transmittance spectra shown in Fig. S5 of the supplementary information. Consequently, we observe the reduction of ER for sample D3. Operational bandwidths in transmission geometry are found nearly the same for D1 and D2 in RB-1 (around $4.5\mu\text{m}$) and RB-2 (around $1.5\mu\text{m}$) spectral region. These operational bandwidths in RB-1 and RB-2 spectral regions for reflection and transmission geometry have been tabulated in Table-1 for samples D1-D3. Similarly, DOP in the proposed bandwidth for transmission geometry is found more than -0.75 and 0.85 in RB-1 and RB-2, respectively, suggesting nearly linear polarized light at the output. In summary, our FTIR studies confirm that α -MoO₃ based IR-polarizer, at optimum thickness, exhibits ER of 7.5dB and 10dB in RB-1 and RB-2 spectral re-

gion, respectively. The DOP in the proposed operational bandwidth is ≥ 0.75 and ≥ 0.85 in RB-1 and RB-2, respectively, which suggest nearly linear polarized light at the output. Optimum thickness of α -MoO₃ for large ER and operational bandwidth is found to be around $2.5\mu\text{m}$ to $3.5\mu\text{m}$.

For the first time to our knowledge, our work explores the above room temperature thermal tolerance of the optical responses of α -MoO₃ thin films. Temperature threshold is a critical parameter for optical devices in the mid-IR since the environment and intense IR sources can induce heating and raise the temperature of the polarizer material. In the mid-IR spectral region, optical phonons govern the optical response of α -MoO₃ and the lifetime of optical phonons typically decreases with the increase in temperature[30]. Hence, an enhancement in the optical losses within the material is expected at elevated temperatures, which may lead to deterioration in device performance. Secondly, at high temperatures, the optical phonon frequencies can also shift [31], which may limit the bandwidth of the device. To ensure the temperature stability of α -MoO₃ thin film, we first perform temperature-dependent x-ray diffraction up to 160°C , which is shown in the Fig. S6 of the supplementary information. We found a maximum of around 0.4% out of plane lattice expansion which is reversible on cool-

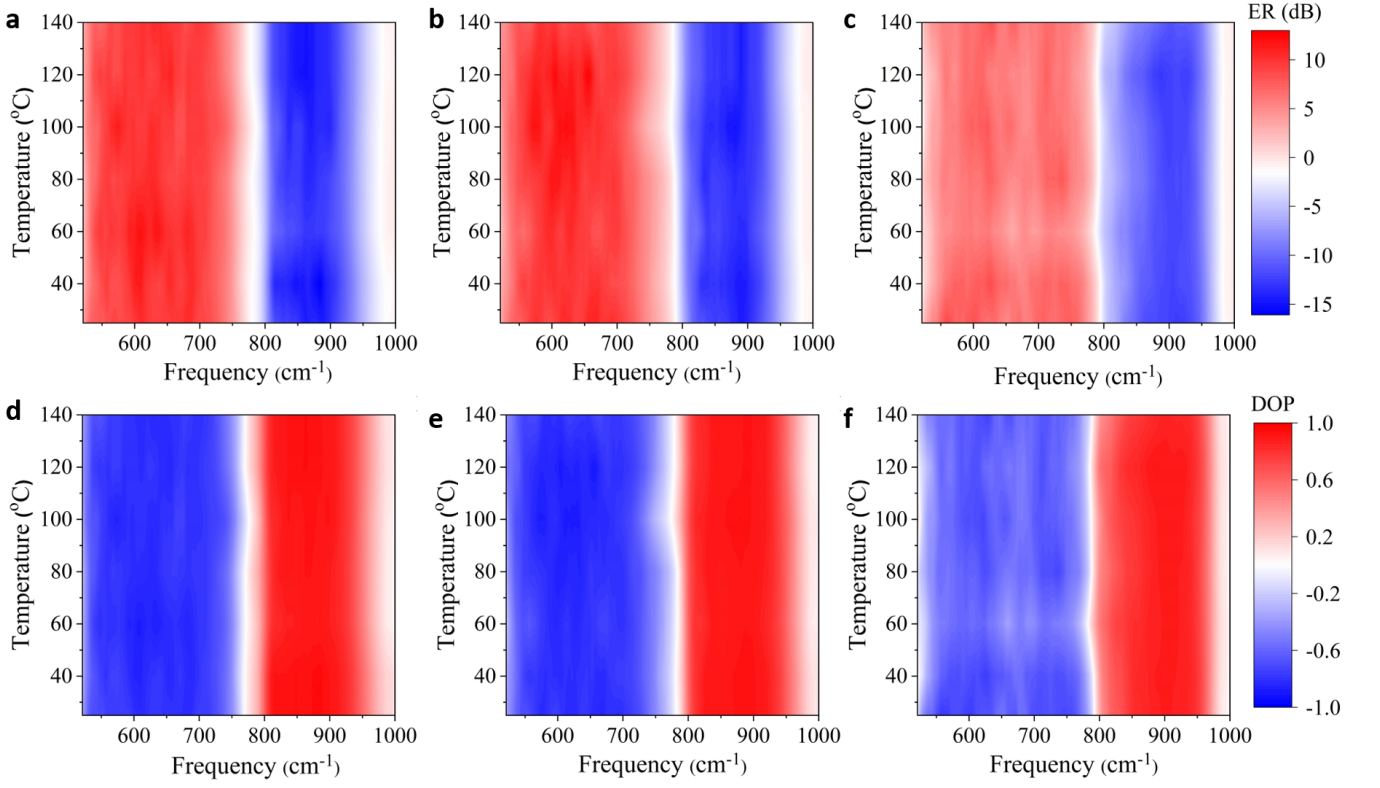


FIG. 5. **Temperature-dependent figures of merit of α -MoO₃ based IR polarizer in transmission geometry.**(a)-(c) show ER as a function of frequency and temperature for thicknesses D1, D2 and D3 respectively. (d)-(f) show DOP as a function of frequency and temperature for thicknesses D1, D2 and D3 respectively.

ing down to room temperature. Subsequently, we perform temperature-dependent polarization-resolved FTIR reflectance and transmittance investigation of samples D1 - D3 for temperature range from 25°C to 140°C. Polarization-resolved reflectance and transmittance of D1-D3 are shown in Figs. S7 and S8 of supplementary information, respectively. We observe only a slight variation in the optical responses when the temperature is increased from 25°C to 140°C, which might be associated with the reduction of phonon lifetimes [30]. Although the observed intensities are nearly constant within 8% - 10% w.r.t. temperature, we have not observed any monotonic trend of intensities. It could be due to the noise resulting from the finite thickness KBr. Furthermore, knife-edge aperture of the FTIR with rough edges might also invoke diffraction-originated noise in the spectrum. These noises mask the expected small variations in the intensities, and hence the presence of any monotonic trend w.r.t. temperature can not be resolved.

Extinction ratio in the reflecting type polarizer as a function of temperature and frequency is shown in Fig. 4(a)-(c) for samples D1 - D3, respectively. We found that ER remains above the threshold values in RB-1 and RB-2 spectral region for the temperature up to 140°C. Furthermore, DOP for samples D1 - D3 are also found nearly similar to room temperature values for tempera-

ture up to 140°C as shown in Fig. 4(d)-(f). Similarly, ER and DOP for samples D1 - D3 of transmission type polarizer are shown in Fig. 5(a)-(c) and Fig. 5(d)-(f), respectively, where ER for D1 and D2 withhold its threshold up to temperature 140°C (Fig. 5(a)-(b)) in RB-1 spectral region. Furthermore, the operational bandwidths in both RBs remains almost similar in the entire temperature range. Since sample D3 exhibits ER below threshold even at room temperature due to the higher α -MoO₃ thickness, ER of this sample also remains below threshold in most of RB-1 spectral region at higher temperatures as shown in Fig. 5(c). Moreover, DOP in the transmission type polarizers for samples D1 and D2 remains more than -0.75 and 0.85 in RB-1 and RB-2, respectively, up to 140°C. From these temperature-dependent FTIR investigations, we conclude that α -MoO₃ thin film based reflecting and transmission type IR polarizers can retain their figures of merit (ER and DOP) up to 140°C while retaining similar operational bandwidths in both RBs. Temperature dependent XRD studies confirm that α -MoO₃ crystal structure can withstand temperature 140°C with a reversible 0.4% of out the plane lattice expansion.

III. CONCLUSION

In this work, we investigated the optical properties of large-scale fabricated single crystal α - MoO_3 films for application towards mid-IR polarizer in reflection and transmission geometry. Our polarization-resolved Raman studies confirm the inherent in-plane anisotropic nature of the synthesized flakes. Polarization properties of α - MoO_3 films in the mid-IR region are attributed to their strong in-plane hyperbolic anisotropy. We found optimum thickness of α - MoO_3 films for efficient mid-IR polarizer to be in the range of $2.5\mu\text{m}$ to $3.5\mu\text{m}$ in which ER is observed to be more than 7.5 dB in RB-1 and more than 10 dB in RB-2 spectral region. Operational bandwidth at optimum thickness is found around $2.75\mu\text{m}$ and $1.0\mu\text{m}$ in RB-1 and RB-2 spectral region, respectively, for reflection type polarizer and around $4.5\mu\text{m}$ and $1.5\mu\text{m}$ in RB-1 and RB-2 spectral region, respectively, for transmission type polarizer. To the best of our knowledge, temperature-dependent studies for the optical response of α - MoO_3 thin films in the mid-IR have been carried out above room temperature for the first time. This study confirms that our proposed α - MoO_3 based polarizer device retains excellent reflectance and transmittance characteristics with a temperature tolerance up to (140°C). This work affirms the potential of sub-wavelength vdW thin film of α - MoO_3 for miniaturized mid-IR optical devices without using any complicated lithography techniques and can be easily integrated onto the chip-scale platform. This study further opens up the application arena of vdW natural hyperbolic crystals for lithography-free alternatives for other exotic optical functionalities such as quantum interference[14], sensing[32], planar hyperlensing, and thermal emission control[33].

IV. EXPERIMENTAL SECTION

Deposition of α - MoO_3 thin films: Fabrication of α - MoO_3 thin films has been carried out here using thermal physical evaporation technique[21] in a two-zone split-furnace as shown schematically in the Fig. 1(a). Briefly, 0.1 gm of MoO_3 powder (Sigma-Aldrich) with a purity of 99.99% has been kept in a cleaned quartz boat at zone-1 (800°C) and a cleaned silicon substrate is kept around 15 cm away at zone-2 (600°C) as shown in the Fig. 1(a). Heating rate for both zones is kept around 10°C per minute. Furnace is kept at target temperature for 120 minutes and then cooled down to room temperature naturally. This process results in the deposition of flakes on a silicon substrate and free-standing thick single-crystal flakes on the wall of the quartz tube. Next, we use the mechanical exfoliation technique of free-standing flakes of α - MoO_3 using scotch-tape to obtain the desired thickness of α - MoO_3 thin film and transfer it on a KBr window, act like substrate in our case, using thermal release tape.

Structural Characterization of α - MoO_3 thin films: HR-TEM and SAED pattern was obtained by FEI Tec-

nai G2, F30 with an acceleration voltage of 300 kV. Temperature-dependent structural properties of α - MoO_3 thin films were studied from Rigaku X-ray diffractometer using $\text{Cu-K}\alpha$ radiation (1.541 \AA), operated at 40 kV of potential and 40 mA of current, in the $2\theta - \omega$ mode with a scan rate of 6 degrees per minute. The samples were heated at a rate of $10^\circ\text{C}/\text{min}$ with 10 min of stay time at target temperature. Morphology of α - MoO_3 thin-films on silicon substrate was observed using JEOL-JSM scanning electron microscope operated at an accelerating voltage of 20kV in the secondary electron mode. X-ray photoelectron spectroscopy (XPS) was carried out using Kratos Analytical, Axis Supra for elemental composition analysis. The spectrometer was calibrated with respect to the binding energy of 1s of carbon at 285.0 eV. Thickness profiles of various deposited and transferred flakes were investigated using Bruker's DekTak XT stylus profilometer. Polarization-resolved Raman spectroscopy was carried out in back-scattering geometry using Horiba's Jobin Yvon Lab-Ram 800 at room temperature. A 532 nm solid-state laser line was used as an excitation source and a 100x long working distance objective with a numerical aperture (NA) of 1.25 was used for focusing the laser beam to a spot size of around $0.5\mu\text{m}$. Raman spectrometer was initially calibrated using Raman active optical mode of crystalline silicon at 520.70 cm^{-1} . An analyzer is placed in the path of back-scattered light before the spectrometer's entrance, which allows us to analyze the Raman shift parallel or perpendicular to incident laser light. Rotation of flake method is adopted using rotational stage keeping the polarization state of incident laser light fixed.

Fourier-Transform Infrared Spectroscopy: Mid-infrared optical response of the α - MoO_3 thin films were studied in the $520\text{ cm}^{-1} - 1000\text{ cm}^{-1}$ spectral region using Bruker Hyperion-3000 FTIR microscope equipped with Bruker Vertex 80 spectrometer. Temperature-dependent studies were carried out upto 140°C with an interval of 20°C using a Hyperion heatable sample holder, and a Pt100 resistor was connected for sensing the current temperature. Temperature control unit uses a digital PID algorithm for controlling the temperature. Stay time at the target temperature was kept at 10 min. The IR light is illuminated using a 15X Cassegrain objective with a NA of 0.40 and an average off-normal incident angle of about 17° . Spectrum is recorded with the help of a wideband MCT (mercury cadmium telluride) detector at the spectral resolution of 2 cm^{-1} and 256 number of scan. Flakes are kept in such a manner that the x-axis of the FTIR instrument is parallel to the [100] direction of α - MoO_3 . The polarization-dependent studies were carried out using a KRS-5 based IR polarizer. Here, reflectance spectra are collected with respect to the gold background in the back-scattering geometry, and transmittance spectra are collected with respect to the air background. A knife-edge aperture is set with an area $90\mu\text{m} \times 130\mu\text{m}$ for the selection of area on α - MoO_3 flake. All FTIR spectra are smoothed by weighted

adjacent averaging from 9 points to remove noises.

Acknowledgement. N.R.S. acknowledges the Council of Scientific & Industrial Research fellowship No: 09/087(0997)/2019-EMR-I. S.D. acknowledges financial support from Institute Postdoctoral Fellowship IIT Bombay. A.K.S. acknowledges Industrial Research and Consultancy Center for the financial support. A.K. ac-

knowledges funding from the Department of Science and Technology via the grants: SB/S2/RJN-110/2017, ECR/2018/001485 and DST/NM/NS-2018/49. We acknowledge Industrial Research and Consultancy Center and the Center for Research in Nanotechnology and Science, IIT Bombay for providing access to characterization facilities.

-
- [1] Weiliang Ma, Pablo Alonso-González, Shaojuan Li, Alexey Y. Nikitin, Jian Yuan, Javier Martín-Sánchez, Javier Taboada-Gutiérrez, Iban Amenabar, Peining Li, Saül Vélez, Christopher Tollan, Zhigao Dai, Yupeng Zhang, Sharath Sriram, Kourosh Kalantar-Zadeh, Shuit-Tong Lee, Rainer Hillenbrand, and Qiaoliang Bao. In-plane anisotropic and ultra-low-loss polaritons in a natural van der waals crystal. *Nature*, 562(7728):557–562, October 2018.
- [2] Javier Taboada-Gutiérrez, Gonzalo Álvarez-Pérez, Jiahua Duan, Weiliang Ma, Kyle Crowley, Iván Prieto, Andrei Bylinkin, Marta Autore, Halyna Volkova, Kenta Kimura, Tsuyoshi Kimura, M.-H. Berger, Shaojuan Li, Qiaoliang Bao, Xuan P. A. Gao, Ion Errea, Alexey Y. Nikitin, Rainer Hillenbrand, Javier Martín-Sánchez, and Pablo Alonso-González. Broad spectral tuning of ultra-low-loss polaritons in a van der waals crystal by intercalation. *Nature Materials*, 19(9):964–968, April 2020.
- [3] Joshua D. Caldwell, Igor Aharonovich, Guillaume Cassabois, James H. Edgar, Bernard Gil, and D. N. Basov. Photonics with hexagonal boron nitride. *Nature Reviews Materials*, 4(8):552–567, July 2019.
- [4] Souvik Biswas, William S. Whitney, Meir Y. Grajower, Kenji Watanabe, Takashi Taniguchi, Hans A. Bechtel, George R. Rossman, and Harry A. Atwater. Tunable intraband optical conductivity and polarization-dependent epsilon-near-zero behavior in black phosphorus. *Science Advances*, 7(2):eabd4623, January 2021.
- [5] Alexander Poddubny, Ivan Iorsh, Pavel Belov, and Yuri Kivshar. Hyperbolic metamaterials. *Nature Photonics*, 7(12):948–957, November 2013.
- [6] Zebo Zheng, Ningsheng Xu, Stefano L. Oscurato, Michele Tamagnone, Fengsheng Sun, Yinzhu Jiang, Yanlin Ke, Jianing Chen, Wuchao Huang, William L. Wilson, Antonio Ambrosio, Shaozhi Deng, and Huanjun Chen. A mid-infrared biaxial hyperbolic van der waals crystal. *Science Advances*, 5(5):eaav8690, May 2019.
- [7] Fengnian Xia, Han Wang, and Yichen Jia. Rediscovering black phosphorus as an anisotropic layered material for optoelectronics and electronics. *Nature Communications*, 5(1), July 2014.
- [8] You-Chia Chang, Che-Hung Liu, Chang-Hua Liu, Siyuan Zhang, Seth R. Marder, Evgenii E. Narimanov, Zhaohui Zhong, and Theodore B. Norris. Realization of mid-infrared graphene hyperbolic metamaterials. *Nature Communications*, 7(1), February 2016.
- [9] Chong Wang, Shenyang Huang, Qiaoxia Xing, Yuangang Xie, Chaoyu Song, Fanjie Wang, and Hugen Yan. Van der waals thin films of WTe₂ for natural hyperbolic plasmonic surfaces. *Nature Communications*, 11(1), March 2020.
- [10] Lei Tong, Xinyu Huang, Peng Wang, Lei Ye, Meng Peng, Licong An, Qiaodong Sun, Yong Zhang, Guoming Yang, Zheng Li, Fang Zhong, Fang Wang, Yixiu Wang, Maithilee Motlag, Wenzhuo Wu, Gary J. Cheng, and Weida Hu. Stable mid-infrared polarization imaging based on quasi-2d tellurium at room temperature. *Nature Communications*, 11(1), May 2020.
- [11] Mai Desouky, M. R. Anisur, Maria Alba, R. K. Singh Raman, Mohamed. A. Swillam, Nicolas H. Voelcker, and Amal Kasry. Near-field mapping of localized plasmon resonances in metal-free, nanomembrane graphene for mid-infrared sensing applications. *ACS Applied Nano Materials*, 1(11):6454–6462, October 2018.
- [12] Kyoung Min Yoo, Jason Midkiff, Ali Rostamian, Chi jui Chung, Hamed Dalir, and Ray T. Chen. InGaAs membrane waveguide: A promising platform for monolithic integrated mid-infrared optical gas sensor. *ACS Sensors*, 5(3):861–869, March 2020.
- [13] Stefano Pirotta, Ngoc-Linh Tran, Arnaud Jollivet, Giorgio Biasiol, Paul Crozat, Jean-Michel Manceau, Adel Bousseksou, and Raffaele Colombelli. Fast amplitude modulation up to 1.5 GHz of mid-IR free-space beams at room-temperature. *Nature Communications*, 12(1), February 2021.
- [14] Muralidhar Nalabothula, Pankaj K Jha, Tony Low, and Anshuman Kumar. Engineering valley quantum interference in anisotropic van der waals heterostructures. *Physical Review B*, 102(4):045416, 2020.
- [15] Sina Abedini Dereshgi, Thomas G. Folland, Akshay A. Murthy, Xianglian Song, Ibrahim Tanriover, Vinayak P. Dravid, Joshua D. Caldwell, and Koray Aydin. Lithography-free IR polarization converters via orthogonal in-plane phonons in α -MoO₃ flakes. *Nature Communications*, 11(1), November 2020.
- [16] Kai Ou, Feilong Yu, Guanhai Li, Wenjuan Wang, Andrey E. Miroshnichenko, Lujun Huang, Peng Wang, Tianxin Li, Zhifeng Li, Xiaoshuang Chen, and Wei Lu. Mid-infrared polarization-controlled broadband achromatic metadvice. *Science Advances*, 6(37):eabc0711, September 2020.
- [17] Joshua D. Caldwell, Igor Vurgaftman, Joseph G. Tischler, Orest J. Glembocki, Jeffrey C. Owrutsky, and Thomas L. Reinecke. Atomic-scale photonic hybrids for mid-infrared and terahertz nanophotonics. *Nature Nanotechnology*, 11(1):9–15, January 2016.
- [18] Seyoon Kim, Sergey G. Menabde, Victor W. Brar, and Min Seok Jang. Functional mid-infrared polaritonics in van der waals crystals. *Advanced Optical Materials*, 8(5):1901194, November 2019.
- [19] Qiushi Guo, Cheng Li, Bingchen Deng, Shaofan Yuan, Francisco Guinea, and Fengnian Xia. Infrared nanophotonics based on graphene plasmonics. *ACS Photonics*, 4(12):2989–2999, August 2017.

- [20] Stephanie Law, Viktor Podolskiy, and Daniel Wasserman. Towards nano-scale photonics with micro-scale photons: the opportunities and challenges of mid-infrared plasmonics. *Nanophotonics*, 2(2):103–130, April 2013.
- [21] Yu Wang, Xiang Du, Jiming Wang, Mingze Su, Xi Wan, Hui Meng, Weiguang Xie, Jianbin Xu, and Pengyi Liu. Growth of large-scale, large-size, few-layered α -moo3 on sio2 and its photoresponse mechanism. *ACS applied materials & interfaces*, 9(6):5543–5549, 2017.
- [22] Bernard Dennis Cullity. *Elements of X-ray Diffraction*. Addison-Wesley Publishing, 1956.
- [23] Xiaxia Liao, Ah Reum Jeong, Regan G. Wilks, Sven Wiesner, Marin Rusu, Roberto Félix, Ting Xiao, Claudia Hartmann, and Marcus Bär. Tunability of MoO3 thin-film properties due to annealing in situ monitored by hard x-ray photoemission. *ACS Omega*, 4(6):10985–10990, June 2019.
- [24] Muqian Wen, Xuexian Chen, Zebo Zheng, Shaozhi Deng, Zhibing Li, Weiliang Wang, and Huanjun Chen. In-plane anisotropic raman spectroscopy of van der waals α -MoO3. *The Journal of Physical Chemistry C*, 125(1):765–773, December 2020.
- [25] L Seguin, M Figlarz, R Cavagnat, and J.-C Lassègues. Infrared and raman spectra of MoO3 molybdenum trioxides and MoO3 · xH2o molybdenum trioxide hydrates. *Spectrochimica Acta Part A: Molecular and Biomolecular Spectroscopy*, 51(8):1323–1344, July 1995.
- [26] Sergio Puebla, Roberto D’Agosta, Gabriel Sánchez-Santolino, Riccardo Frisenda, Carmen Munuera, and Andres Castellanos-Gomez. In-plane anisotropic optical and mechanical properties of two-dimensional moo3. *npj 2D Materials and Applications*, 5, 12 2021.
- [27] Gonzalo Álvarez-Pérez, Thomas G Folland, Ion Errea, Javier Taboada-Gutiérrez, Jiahua Duan, Javier Martín-Sánchez, Ana IF Tresguerres-Mata, Joseph R Matson, Andrei Bylinkin, Mingze He, et al. Infrared permittivity of the biaxial van der waals semiconductor α -moo3 from near-and far-field correlative studies. *Advanced Materials*, 32(29):1908176, 2020.
- [28] COMSOL. Comsol multiphysics reference manual, version 5.5. www.comsol.com, May 2020.
- [29] Saurabh Dixit, Nihar Ranjan Sahoo, Abhishek Mall, and Anshuman Kumar. Mid infrared polarization engineering via sub-wavelength biaxial hyperbolic van der waals crystals. *Scientific reports*, 11(1):1–9, 2021.
- [30] Jose V Silveira, Luciana L Vieira, Josue Mendes Filho, Antonio JC Sampaio, Oswaldo L Alves, and Antonio G Souza Filho. Temperature-dependent raman spectroscopy study in moo3 nanoribbons. *Journal of Raman spectroscopy*, 43(10):1407–1412, 2012.
- [31] Siqi Zhu and Wei Zheng. Temperature-dependent phonon shifts in van der waals crystals. *The Journal of Physical Chemistry Letters*, 12(22):5261–5270, June 2021.
- [32] Giovanna Palermo, Kandammathe Valiyaveedu Sreekanth, Nicolò Maccaferri, Giuseppe Emanuele Lio, Giuseppe Nicoletta, Francesco De Angelis, Michael Hinczewski, and Giuseppe Strangi. Hyperbolic dispersion metasurfaces for molecular biosensing. *Nanophotonics*, 10(1):295–314, October 2020.
- [33] J. S. Gomez-Diaz and Andrea Alù. Flatland optics with hyperbolic metasurfaces. *ACS Photonics*, 3(12):2211–2224, December 2016.